ARTICLE INFO
Article ID: 10-04-02-0013
© 2020 Vanliem Nguyen, Renqiang Jiao, Jianrun Zhang
doi:10.4271/10-04-02-0013

Control Performance of Damping and Air Spring of Heavy Truck Air Suspension System with Optimal Fuzzy Control

Vanliem Nguyen,[1] Renqiang Jiao,[1] and Jianrun Zhang[2]

[1]Hubei Polytechnic University, China
[2]Southeast University, China

Abstract

The air suspension system of heavy trucks not only improves the vehicle's ride comfort but also reduces the negative impact on the road surface. In order to evaluate the performance of the control damping (CD) and the control air spring (CAS) of the vehicle air suspension system on the ride comfort and the road friendliness, a three-dimensional (3D) nonlinear dynamic model with 14 degrees of freedom (DOF) of the heavy trucks and optimal fuzzy control (OFC) with control rules optimized by the genetic algorithm (GA) are proposed in this study. The root mean square (RMS) acceleration response of the tractor and the dynamic load coefficient (DLC) at the wheel axles are chosen as objective functions under the various operating conditions. Contrastive analysis of the RMS and DLC values with the passive (P), CD, and CAS methods of the air suspension system is carried out respectively. The research result shows that both the CD and CAS methods remarkably improve the ride comfort and road friendliness of the heavy trucks in comparison with P, especially the CAS method has an obvious effect on mitigating the road damage in comparison with the CD method; conversely the CD method is better than the CAS method to improve the tractor's ride comfort under different operating conditions.

History

Received: 09 Jul 2019
Revised: 09 Dec 2019
Accepted: 28 Jan 2020
e-Available: 28 Feb 2020

Keywords

Heavy truck, Dynamic load coefficient, Air suspension system, Optimal fuzzy control, Ride comfort

Citation

Nguyen, V., Jiao, R., and Zhang, J., "Control Performance of Damping and Air Spring of Heavy Truck Air Suspension System with Optimal Fuzzy Control," *SAE Int. J. Veh. Dyn., Stab., and NVH* 4(2):179-194, 2020, doi:10.4271/10-04-02-0013.

ISSN: 2380-2162
e-ISSN: 2380-2170

© 2020 Vanliem Nguyen, Renqiang Jiao, Jianrun Zhang. Published by SAE International. This Open Access article is published under the terms of the Creative Commons Attribution License (http://creativecommons.org/licenses/by/4.0/), which permits distribution, and reproduction in any medium, provided that the original author(s) and the source are credited.



1. Introduction

The air suspension system has been studied and applied for the vehicles to improve the ride comfort, especially commercial vehicles [1, 2, 3, 4, 5, 6, 7]. The performance of three different suspension systems including steel leaf, steel spring, and air spring was analyzed and compared in reducing the DLC of tire forces and improving the ride comfort of the vehicles [4, 7, 8]. A 3D air spring model with friction and orifice damping [5] studied for the train projects was then applied for the cab's isolation system of the vibratory roller to increase the ride comfort [6]. Research results showed that the air suspension system not only improved the ride comfort but also significantly reduced the road damage in comparison with other suspension systems as steel leaf, steel spring, or rubber mount [4, 6].

Nowadays, due to the demand for transport development, all vehicles need to travel safer, at a higher speed, and with more stability and road friendliness, particularly the heavy trucks. In order to solve this problem, the air suspension system of heavy trucks was also studied and controlled [1, 2, 3, 9]. A half heavy truck air suspension system model with the Fuzzy-proportional-integral-derivative (PID) controller was researched to control the damping coefficient of the magneto-rheological (MR) fluid [1, 2, 10, 11, 12, 13], a 3D heavy truck model using air suspension system was also established, semi-active fuzzy control was then developed to control the damping coefficient of the air suspension system [3]. Besides a quarter heavy truck model used air suspension system was also built, and the stiffness coefficient of the air spring was then controlled based on fuzzy control [9]. The RMS acceleration response of the vehicles was chosen as the objective function of the studies. The research result showed that both the CD and CAS methods of the air suspension system significantly improved the vehicle's ride comfort. Additionally, in the above researches, the road friendliness of heavy trucks using semi-active air suspension system was significantly improved based on the evaluating criteria of the reducing tire loads [1], the DLC [3], and road damage coefficient [9]. Also on these evaluating criteria, the DLC value was commonly used to evaluate the performance of suspension systems on the road damage [4, 8, 14]. However, the performance of the air suspension system using the CD method or CAS method to improve the ride comfort and road friendliness of heavy trucks has not yet been evaluated.

In addition, to enhance the control performance of the semi-active suspension system using the MR fluid mount [12, 13], the optimal control methods, such as Neuro-Fuzzy control with the fuzzy rules optimized by the GA [15], Fuzzy-PID control with the control rules optimized by cultural algorithm or GA [10, 16], or Fuzzy-skyhook control using the multi-objective microgenetic algorithm [17], were successfully applied. The results showed that the optimal control methods were better than without optimization. However, the quarter car models with the damping coefficient of the MR fluid were mostly applied and controlled for all the researches. The optimal control methods have not yet been considered and developed to control the stiffness coefficient of air spring mount of the vehicles equipped with air suspension system, especially the heavy trucks.

In this study, a 3D nonlinear dynamic model with 14 DOF of the heavy trucks equipped with the air suspension system is established under the different operating conditions. The fuzzy logic control with the control rules optimized by GA is developed based on MATLAB software, and it is then applied to control the damping or air spring of the air suspension system. Both the RMS and DLC values of the tractor and wheel axles are chosen as objective functions. The performance of the CD and CAS methods are evaluated based on objective functions when the vehicle travels on various operating conditions.

The scientific contribution of this article is that a 3D dynamic model of five-axle heavy trucks that fully reflects the vehicle's pitch and roll vibrations is researched. A new optimal control method of the fuzzy logic control based on the multi-objective optimal program of GA is successfully studied to control the damping and air spring of the air suspension system. The research result shows that heavy truck's air suspension system using the CD method improve better ride comfort in comparison with both the P and CAS method; conversely the CAS method is better than both the P and CAS method to improve the road friendliness under different operating conditions.

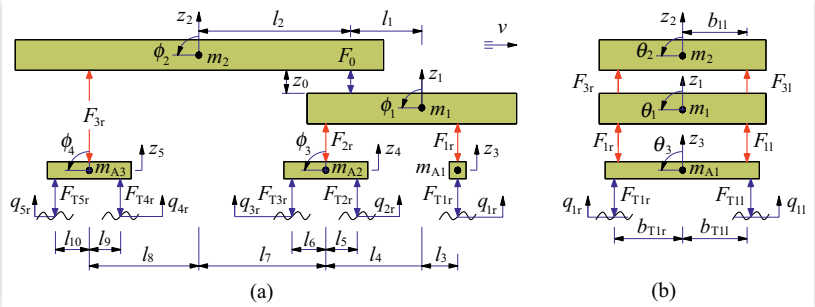
2. Heavy Truck Model

2.1. Vehicle Dynamic Model

An air suspension system of five-axle heavy trucks with a dependent suspension system for the front axle and a walking beam suspension system for the rear axles is chosen to analyze the vehicle dynamic. A 3D nonlinear dynamic model of the vehicle with 14 DOF is then established to evaluate the performance between the CD and CAS methods of the air suspension system. The vehicle model is shown in Figure 1.

where F_{in} is the vertical dynamic force of the air suspension system at the front, middle, and rear axles; F_{Tjn} is the vertical dynamic force of tires; F_0 is the vertical dynamic force of the articulation connection between the tractor driver and trailer; m_1 and m_2 are the sprung mass of the tractor and trailer; m_{Ai} is the unsprung mass of the front axle, the first tandem axle, and the second tandem axle; z_j, ϕ_k, and θ_j are the vertical and angular displacements at center of gravity of the tractor, trailer, and axles; q_{jn} is the excitation of the road surfaces; l_α and b_δ is the distance of the vehicle ($i = 1, 2, 3, j = 1, 2, \ldots, 5, n = \mathrm{r}, \mathrm{l}, k = 1, 2, 3, 4, \alpha = 1, 2, \ldots, 10$, and $\delta = 1, 2$).

FIGURE 1 A dynamic model of the heavy trucks with (a) side view and (b) front view.



© Vanliem Nguyen, Renqiang Jiao, Jianrun Zhang

Based on the vehicle dynamic model, as shown in Figure 1, and by applying Newton's second law of motion of the force and moment equations, the general dynamic differential equation of the vehicle are written as follows:

$$
\begin{aligned}
&m_1\ddot{z}_1 = F_{1r} + F_{1l} + F_{2r} + F_{2l} - F_0,\\
&I_{1y}\ddot{\phi}_1 = -\left(F_{1r} + F_{1l}\right)l_3 + \left(F_{2r} + F_{2l}\right)l_4 - F_0 l_1,\\
&I_{1x}\ddot{\theta}_1 = \left(F_{1r} + F_{2r}\right)b_{1r} - \left(F_{1l} + F_{2l}\right)b_{1l},\\
&m_2\ddot{z}_2 = F_{3r} + F_{3l} + F_0,\\
&I_{2y}\ddot{\phi}_2 = \left(F_{3r} + F_{3l}\right)l_8 - F_0 l_2,\\
&I_{2x}\ddot{\theta}_2 = F_{3r}b_{3r} - F_{3l}b_{3l},\\
&m_{A1}\ddot{z}_3 = -F_{1r} - F_{1l} + F_{T1r} + F_{T1l},\\
&I_{3x}\ddot{\theta}_3 = -F_{1r}b_{1r} + F_{1l}b_{1l} + F_{T1r}b_{T1r} - F_{T1l}b_{T1l},\\
&m_{A2}\ddot{z}_4 = -F_{2r} - F_{2l} + F_{T2r} + F_{T2l} + F_{T3r} + F_{T3l},\\
&I_{4y}\ddot{\phi}_3 = -\left(F_{T2r} + F_{T2l}\right)l_5 + \left(F_{T3r} + F_{T3l}\right)l_6,\\
&I_{4x}\ddot{\theta}_4 = -F_{2r}b_{1r} + F_{2l}b_{1l} + (F_{T2r} + F_{T3r})b_{T1r} - (F_{T2l} + F_{T3l})b_{T1l},\\
&m_{A3}\ddot{z}_5 = -F_{3r} - F_{3l} + F_{T4r} + F_{T4l} + F_{T5r} + F_{T5l},\\
&I_{5y}\ddot{\phi}_4 = -\left(F_{T4r} + F_{T4l}\right)l_9 + \left(F_{T5r} + F_{T5l}\right)l_{10},\\
&I_{5x}\ddot{\theta}_5 = -F_{3r}b_{1r} + F_{3l}b_{1l} + (F_{T4r} + F_{T5r})b_{T1r} - (F_{T4l} + F_{T5l})b_{T1l},
\end{aligned}
\qquad \text{Eq. (1)}
$$

The articulation connection between the tractor and trailer is more like a clearance spring attributed to the separation of the fifth wheel plates, and it is used not only to guide the trailer and transverse stability but also to reduce the vibration transmission from the tractor to the trailer. It is modeled as a linear spring with high stiffness and low damping coefficients (K_0 and C_0) [2, 3, 18]. With the linear articulation model, it can be used to determine the dynamic reaction force of the articulation connection in the vertical direction; conversely, the limitation of the linear articulation model is that it cannot apply to study the effect of lateral forces and the vehicle's transverse stability when the vehicle travels on a curve or a turn. However, in this study, the dynamic reaction force of the articulation connection is only considered in the vertical direction; thus, the linear articulation model is applied to determine the dynamic reaction force of the articulation connection, and its equation is described by

$$F_0 = C_0\dot{z}_0 + K_0 z_0 \qquad \text{Eq. (2)}$$

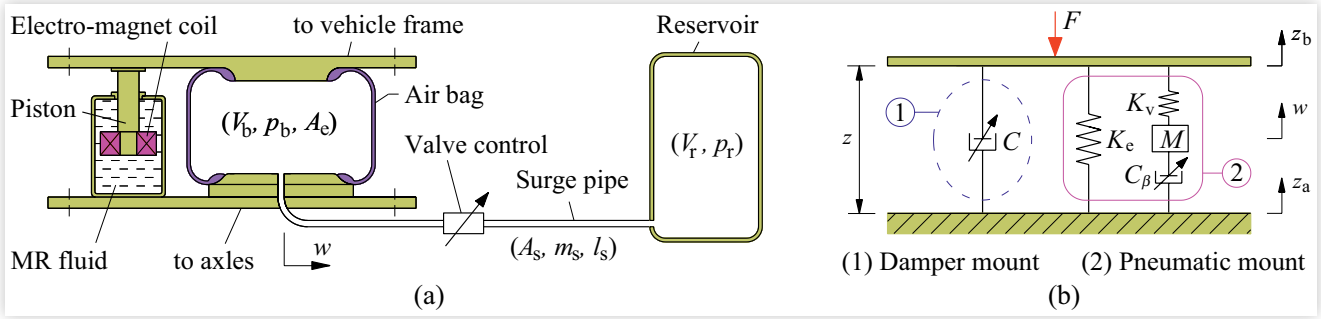
The vertical dynamic force of the air suspension system on the axles (F_{in}) and of the right and left tires (F_{Tjn}) are determined in Sections 2.2 and 2.3, respectively.

2.2. Control Model of the Air Suspension System

To compare the performance between the CD and CAS methods of the air suspension system, three different air suspension structures including the passive air suspension system (P), air suspension system with the CD, and air suspension system with the CAS are proposed in Figure 2a as follows.

1. For the P, its structure includes a passive damping piston of the damper mount and passive air spring mount.
2. For the CD, its structure includes a damping piston controlled by the MR fluid of the damper mount and a passive air spring mount. The damping piston is equipped with a flux guide and an electromagnet coil. When the current in the electromagnet coil is changed based on the control signals, the magnetic field in the flux guide is also altered, so the viscosity of the MR fluid passing through the annular orifice is changed. The result is that the damping force of the damper mount can be controlled according to the excitation of the road surface [10, 12].
3. For the CAS, its structure also includes a passive damping piston of the damper mount and an air spring which is controlled. In the air spring system, an air bag is connected to an air reservoir via a surge pipe and valve control, the stiffness of air bag can be changed and depended on the control of the valve in the surge pipe. According to the GENSYS model of the pneumatic mount [6], the control model of the air suspension system is described as in Figure 2b.

FIGURE 2 (a) Simple structure model of the air suspension system and (b) its control model.



© Vanliem Nguyen, Renqiang Jiao, Jianrun Zhang

where $z = z_a - z_b$ is the relative displacement of the air suspension, K_e and K_v are the static and viscous stiffness constants, M is the mass of the air in the air bag, C_β and w are the nonlinear damping coefficient and displacement of the air in the surge pipe, and C is the damping coefficient of MR fluid which is written by

$$C = \begin{cases} C_p & \text{Passive damping coefficient} \\ C_{ctrl} & \text{Control damping coefficient} \end{cases} \quad \text{Eq. (3)}$$

The vertical dynamic force of the air suspension system in Figure 2b is described by $F = F_D + F_A$, herein F_D and F_A are the damping and elastic forces of the damper and air spring mounts. The vertical dynamic force of F_D is determined by

$$F_D = \begin{cases} C_p \dot{z} & \text{Passive damping force} \\ C_{ctrl} \dot{z} & \text{Control damping force} \end{cases} \quad \text{Eq. (4)}$$

Besides the vertical dynamic force of F_A is also determined as follows.

The mechanical behavior in the air bag is very complicated, and it is mainly determined by the characteristic parameter of the pressure, temperature, volume, mass, density, and energy of the air as well as the shape of the air bag based on fluid dynamic and thermodynamic mechanisms. According to the calculation method of a simple air spring mount [7], assuming that the air bag is deformed in the vertical direction z, after the deformation, the new air bag volume V_b and the new reservoir volume V_r with the polytropic process are

$$V_b = V_{b0} - A_e z + A_s w \quad \text{and} \quad V_r = V_{r0} - A_s w \quad \text{Eq. (5)}$$

where V_{b0} and V_{r0} are the initial volumes of the air bag and reservoir, A_e is the effective area of air bag, and A_s is the cross-sectional area of the pipeline.

According to the air suspension model, as illustrated in Figure 2b, the static stiffness constant K_e, viscous stiffness constant K_v, and mass M are respectively determined by [19]

$$K_e = \frac{\lambda p_0 A_e^2}{V_{b0} + V_{r0}}, \quad K_v = K_e \frac{V_{r0}}{V_{b0}}, \quad \text{and}$$
$$M = A_s l_s \rho \left(\frac{A_e}{A_s} \frac{V_{r0}}{V_{b0} + V_{r0}} \right)^2 \quad \text{Eq. (6)}$$

where λ is the polytropic rate ($1 < \lambda < 1.4$), p_0 is the initial pressure in the air bag, l_s is the length of the surge pipe, and ρ is the air density.

The nonlinear viscous damping C_β is only related to the velocity over of the damper; therefore the vertical viscous force F_v is expressed by [5]

$$F_v = K_v (z - w) = C_\beta |\dot{w}|^\beta \, sign(\dot{w}) + M\ddot{w} \quad \text{Eq. (7)}$$

The nonlinear viscous damping C_β is described by

$$C_\beta = \begin{cases} C_t \chi^{1+\beta} & \text{Passive air spring} \\ (C_t + C_{t-ctrl}) \chi^{1+\beta} & \text{Control air spring} \end{cases} \quad \text{Eq. (8)}$$

where $C_t = 0.5\rho A_s (C_f + C_e + C_c + C_b)$ is total loss coefficient due to friction C_f, enlargement C_e, contraction C_c, and bends C_b in the pipe, $C_{t\text{-}ctrl} = 0.5\rho A_s C_{v\text{-}ctrl}$ in which $C_{v\text{-}ctrl}$ is the loss coefficient due to the valve control in the pipe, and $\chi = (A_e/A_s)(V_{r0}/(V_{b0} + V_{r0}))$.

The corresponding dynamic force of the air spring mount in the vertical direction is written by

$$F_A = F_e + F_v = K_e z + C_\beta |\dot{w}|^\beta \, \text{sign}(\dot{w}) + M\ddot{w} \quad \text{Eq. (9)}$$

By combining Equations 4 and 8-9, the control force of the air suspension system is rewritten as follows:

$$F = F_D + F_A = \begin{cases} C_p \dot{z} + K_e z + C_t \chi^{1+\beta} |\dot{w}|^\beta \, \text{sign}(\dot{w}) + M\ddot{w} & \text{With P} \\ F_{D-ctrl} + K_e z + C_t \chi^{1+\beta} |\dot{w}|^\beta \, \text{sign}(\dot{w}) + M\ddot{w} & \text{With CD} \\ C_p \dot{z} + K_e z + C_t \chi^{1+\beta} |\dot{w}|^\beta \, \text{sign}(\dot{w}) + M\ddot{w} + F_{A-ctrl} & \text{With CAS} \end{cases} \quad \text{Eq. (10)}$$

where $F_{D-ctrl} = C_{ctrl} \dot{z}$ and $F_{A-ctrl} = C_{t-ctrl} \chi^{1+\beta} |\dot{w}|^\beta \, \text{sign}(\dot{w})$ are the control forces of the RM fluid and air spring that are controlled by the fuzzy logic controller (FLC) via the CD coefficients of the C_{ctrl} and $C_{t\text{-}ctrl}$, respectively.

Equation 10 is then applied to determine the vertical dynamic force (F_{in}) of the air suspension system on the wheel axles.

2.3. Tire Dynamic Model

When the vehicle travels on the road, the effect of the deformable road surface on the vehicle ride comfort is negligible, and the road surface can be considered as a rigid road. Six types of the tire-rigid road contact models including the point contact, roller contact, fixed footprint contact, radial spring contact, flexible ring contact, and finite element contact were carried out to research the tire dynamic forces under the condition of the vehicle travelling on the road surface roughness [20, 21], as shown in Figure 3a.

For the contact point model, the tire is simplified into a parallel suspension structure where the upper end is connected to the vehicle axle and the lower end is located at the contact point between the tire and road surface. This can convert the roughness of the road surface to vertical force as a vertical excitation of the vehicle. This model can be used to determine the vertical tire dynamic [20]. The disadvantage of this model is that it is difficult to determine the horizontal force of the tire to the change of the roughness of the road surface. In previous researches on the vehicle ride comfort, the tire dynamic was mainly considered in the vertical direction, whereby the contact point model was mostly applied [1, 2, 3, 6, 10, 18, 22]. In this study, the tire dynamic force is mainly determined in the vertical direction, thus the contact point model of the tire-road surface interaction is also applied.

Based on the contact point model and elastic deformation characteristic of the tire, the tire's response in the vertical direction can be described by two stages including the compression process (static and dynamic compressions) and recovery process (tire off-road and tire recovery phases). Based on the quarter vehicle model [18], the nonlinear characteristic of the tire-road surface interaction is illustrated as in Figure 3b-d.

where C_T and K_T are the damping and stiffness coefficients of the tire, m_T is the static mass of the vehicle distributed on the wheel, and g is the gravitational acceleration.

Based on the tire dynamic model in Figure 3b-d, the spring and damping dynamic forces of the tire is determined by

$$F_{K_T} = \begin{cases} K_T(q_T - z_T) & (q_T - z_T) - m_T g / K_T \geq 0 \\ 0 & (q_T - z_T) - m_T g / K_T < 0 \end{cases} \quad \text{and}$$

$$F_{C_T} = C_T(\dot{q}_T - \dot{z}_T) \qquad \text{Eq. (11)}$$

Therefore, the vertical dynamic force of tire is given by

$$F_T = F_{K_T} + F_{C_T} \qquad \text{Eq. (12)}$$

Equation 12 is then used to simulate the nonlinear characteristic of the tire and solve the vertical dynamic reaction force F_{Tjn} at the right and left tires.

3. Vibration Excitation and Evaluating Criteria

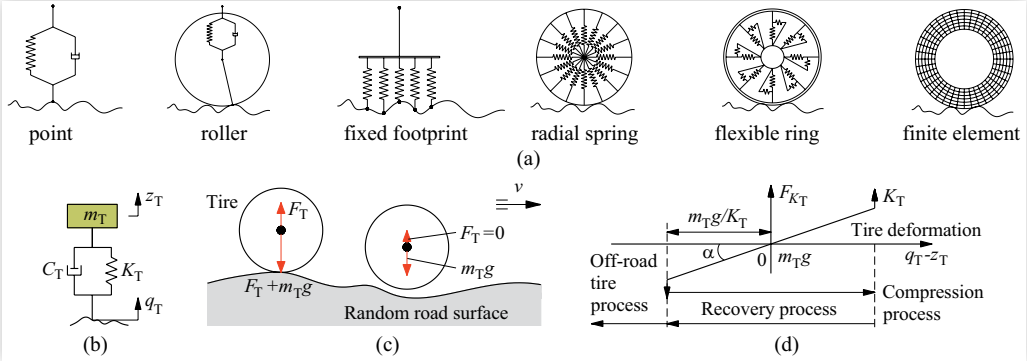
3.1. Vibration Excitation Sources

To compare the performance between the CD and CAS methods, two types of vibration excitation including the random and bumpy road surfaces are respectively considered as follows:

Random road surface: The road surface profile plays an important role to evaluate the performance of the air suspension system. For the random road surface input model, the white noise speed spectrum represented with a realization of a random process via its frequency spectrum density (FSD) is applied to describe the random road in the time domain. The FSD equation of the random road in the time domain can be expressed as [16]

$$S(f) = \frac{1}{v} S(n_0) \left(\frac{n}{n_0} \right)^{-2} = S(n_0) n_0^2 \frac{v}{f^2} \qquad \text{Eq. (13)}$$

FIGURE 3 (a) Tire-rigid road surface contact models, (b) point contact model of the tire-road surface, (c) tire moving on the road surface, and (d) tire's elastic characteristic.



© Vanliem Nguyen, Renqiang Jiao, Jianrun Zhang

where $S(n_0)$ is the road roughness power spectrum density (PSD) and its value is chosen depending on the road condition with the reference spatial frequency $n_0 = 0.1$ m, n is the spatial frequency that represents per meter length of wave number, and f and v are the frequency and vehicle velocity, respectively.

According to the random road using white noise signal in Refs. [1, 16, 23], the random road excitation $q(t)$ is given by

$$\dot{q}(t) + \gamma v^2 q(t) = \gamma \sqrt{S(n_0) v}\, w(t) \qquad \text{Eq. (14)}$$

where $\gamma = 2\pi n_0$ is the spatial frequency of the road surface and $w(t)$ is the random signal of the white noise. The height of the road surface $q(t)$ is determined via the PSD of $S(n_0)$, in which the PSD of the classification of road surface roughness is chosen according to ISO 8068 [24].

The road excitation of the left and right front wheels $q_{1l}(t)$ and $q_{1r}(t)$ can be described by

$$\dot{q}_{11}(t) + \gamma v^2 q_{11}(t) = \gamma \sqrt{S(n_0) v}\, w_{11}(t)$$
$$\text{and } \dot{q}_{1r}(t) + \gamma v^2 q_{1r}(t) = \gamma \sqrt{S(n_0) v}\, w_{1r}(t) \qquad \text{Eq. (15)}$$

According to the vehicle velocity v, the time delay of the left and right wheels j relative to the left and right front wheels are $\Delta t_j = L_j/v$; herein L_j is the distance of the contact points of the left and right wheels j and left and right front wheels (j = 2-5). Therefore, the road excitations of the left and right wheels j are

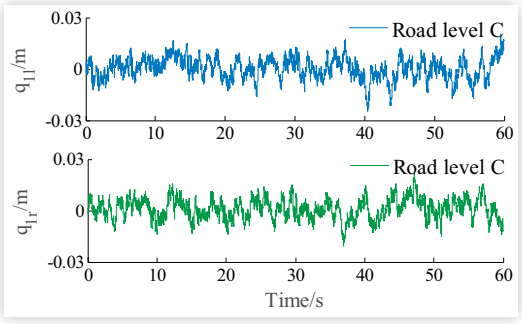
$$q_{j1}(t) = q_{11}(t + \Delta t_j) \quad \text{and} \quad q_{jr}(t) = q_{1r}(t + \Delta t_j) \qquad \text{Eq. (16)}$$

According to ISO 8068 [24], the PSD of road surface roughness is classified as road levels A, B, C, D, E, and H. Thus, in this study, the PSD of road surface roughness of levels B, C, D, and D is also chosen to simulate the system model. By MATLAB/Simulink, the typically random road surfaces $q_{1l}(t)$ and $q_{1r}(t)$ of road level C with $v = 20$ m·s^{-1}, sampling time interval of 0.005 s, and simulation time of 60 s are shown in Figure 4.

Bumpy road surface: The bumpy road surface can be mathematically described by [15]

$$q(t) = \begin{cases} q_0\left(1 - \cos(\omega t)\right) & 1 \le t \le 2 \\ 0 & \text{else} \end{cases} \qquad \text{Eq. (17)}$$

FIGURE 4 Random road surfaces $q_{1l}(t)$ and $q_{1r}(t)$.



© Vanliem Nguyen, Renqiang Jiao, Jianrun Zhang

where $\omega = 2\pi v/L$ in which v is the vehicle speed, and L and q_0 are the bump width and half of the bump height, respectively. To describe $q(t)$, assume that the vehicle travels at a constant velocity of 3 km·h^{-1} on a bump with $q_0 = 0.07$ and $L = 0.85$ m.

3.2. Evaluating Criteria

The performance of suspension systems is often evaluated through three main indexes including the ride comfort, suspension deformation, and road friendliness. For the suspension system of heavy trucks, the ride comfort and road friendliness are two main indexes for evaluating performance. The ride comfort is often reflected via the vertical RMS value of the absolute acceleration of the vehicle body [6]. However, the pitch and roll vibrations of the vehicle body also affect ride comfort [25]. In this study, the performance of the air suspension system with the CD and CAS methods is evaluated via the RMS acceleration response of the vertical, pitch, and roll vibrations at the center of gravity of the tractor, thus the smaller RMS value means to be the better ability of the air suspension system with the corresponding control method. The expression of the RMS value was given by [6, 10, 25]

$$\text{RMS}_l = \sqrt{\frac{1}{T}\int_0^T \left[a_l(t)\right]^2 dt} \qquad \text{Eq. (18)}$$

where subscript l refers to the z_1, ϕ_1, or θ_1 of the vertical, pitch, or roll vibrations at the center of gravity of the tractor and $a_l(t)$ is the acceleration response (translational and rotational) depending on the time of measurement T.

Besides the impact of tire dynamic load on the road surface would lead to stress and strain on the road surface. The long-term accumulation of road surface plastic deformation could cause to destroy the roads, such as cracking and rutting. The tire dynamic load was strongly depended on the vehicle velocity, suspension design, and road roughness [26]. In this problem, many researchers had also given other indicators such as impact factor (IM %) [22], load-sharing criterion [27], and dynamic load-stress factor [18] to evaluate the road friendliness. However, it still has to be calculated through the tire dynamic load (F_T). Therefore, the effect of tire dynamic load on the road surface characterized by the DLC [22, 28] is chosen to evaluate the road friendliness of heavy trucks as follows:

$$\text{DLC}_j = \frac{F_{\text{T}j,\text{RMS}}}{F_{j,\text{st}}} \qquad \text{Eq. (19)}$$

where $F_{\text{T}j,\text{RMS}}$ is the RMS of the tire dynamic load and $F_{j,\text{st}}$ is the corresponding static load of the wheel axle j. The DLC value was in the range from 0.05 to 0.3 under normal operation conditions; it could reduce to zero when the wheel moved on a special smooth road or increased up to 0.4 when the wheel-road contact was broken [3, 8, 14]. In addition, based on Refs. [3, 8], the DLC limiting value of 0.3 was used to evaluate the road friendliness limit of heavy trucks. The DCL value below 0.3 meant the road friendliness; conversely, the DCL value above 0.3 meant the road unfriendliness of heavy

trucks. In this study, the DLC value is also used to evaluate the performance of the air suspension system with the CD and CAS methods on the road friendliness of heavy trucks. Therefore, the lower DLC value means the better ability of the air suspension system with the corresponding control method.

4. Design of the OFC

4.1. The Fuzzy Logic Controller

The FLC created by Zadeh in 1965 has been widely applied in various situations and fields. The FLC does not depend on designed operating conditions, but it only depends on the appropriate selection of the fuzzy inference system (FIS). However, the FIS is almost given by the designer's knowledge and experience [3, 9], so the shortcomings of the FLC are low precision and stability. To solve this problem, this article has developed the optimal control rules for FIS based on the GA program.

In the heavy truck's suspension system model, there are six air suspension systems that should be separately controlled and, thus, six OFC should be designed. However, the design process of these controls is the same, so a specific of the OFC is designed to control the damping coefficient of MR fluid (C_{ctrl}) or nonlinear viscous damping coefficient in the surge pipe via the valve control of the air spring system ($C_{t\text{-}ctrl}$), as depicted in Figure 5. Herein, the FLC's input/output include two input variables denoted by the vertical displacement error (E) and vertical velocity error (EC) of the air suspension system and an output variable denoted by the CD coefficient (u) in which $u = C_{ctrl}$ for the CD or $u = C_{t\text{-}ctrl}$ for the CAS. The vertical dynamic force of the air suspension system F is then decided via the subsystem of the vehicle. In order to enhance the performance of the FLC, the GA is applied to optimize the control rules in FIS via the subsystem and the objective functions.

The next step is the design of FLC. The FLC's structure includes Fuzzification interface, FIS, and Defuzzification interface. First, the crisp value in Fuzzification is transformed into the linguistic variable, FIS is then used by control rules, and finally, the linguistic variable is transformed back to crisp value through Defuzzification for use by the physical plant [29]. Therefore, the FLC can be designed in three steps below.

1. Choosing the FLC's input/output: Two input variables of E and EC are belonging to [−0.1, 0.1] and [−1, 1], and an output variable of u is calibrated over the interval $[0, u_{i\,max}]$. The linguistic variable of two inputs are defined by the positive big (PB), positive small (PS), zero (ZO), negative small (NS), and negative big (NB), and linguistic variable of the output variable is defined as small (S), medium small (MS), medium (M), medium big (MB), and big (B), respectively.
2. Membership function: The shape of membership functions of input/output variables is used by the Triangular function, and its degree of membership is between 0 and 1, as shown in Figure 6.
3. The FIS rules: The initial control rules are given by the designer's knowledge and experience as follows:
   R_i. If E is A_i and EC is B_i, then u_i is D_i ($i = 1, 2, \ldots, 25$).

The FIS is selected by the minimum function and centroid method of Mamdani [29], and the above control rules are then optimized by the GA program through the subsystem model.

4.2. Optimization of the Control Rules Based on GA

GA is an optimal method based on natural selection principles. The goal of GA is to seek the maximum or minimum value of one or more objective functions using computational techniques motivated by biological reproduction. Thus the GA is defined as finding a vector of decision variables satisfying constraints to give acceptable to all objective functions as follows [30, 31]:

Finding the vector $x = [x_1, x_2, \ldots, x_n]^T$ to optimize the objective functions

$$G(x) = \left[g_1(x), g_2(x), \ldots, g_n(x)\right]^T$$
$$\text{Subject to } k_i(x) \le 0,\ i = 1,2,\ldots,P \quad \text{and} \quad h_j(x) = 0,\ j = 1,2,\ldots,Q \qquad \text{Eq. (20)}$$

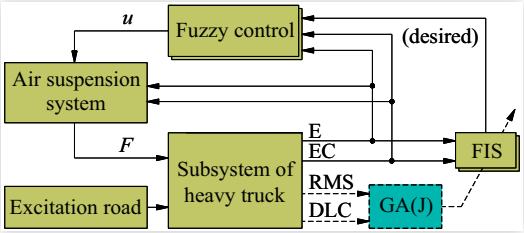
where $G(x)$ is the vector of objective functions, which must be either maximized or minimized, and P and Q are numbers of inequality constraints and equality constraints.

The GA's structure includes the following steps: encoding, population initialization, fitness evaluation, parent selection, genetic operations (crossover and mutate), and termination criterion (Table 1). The flowchart of GA applied for the OFC is built as in Figure 7.

The GA is mainly applied to seek the optimal control rules in FIS to get the minimum value of both RMS and DCL values via the subsystem model in Figure 5. Therefore, the optimal process of GA includes the following steps:

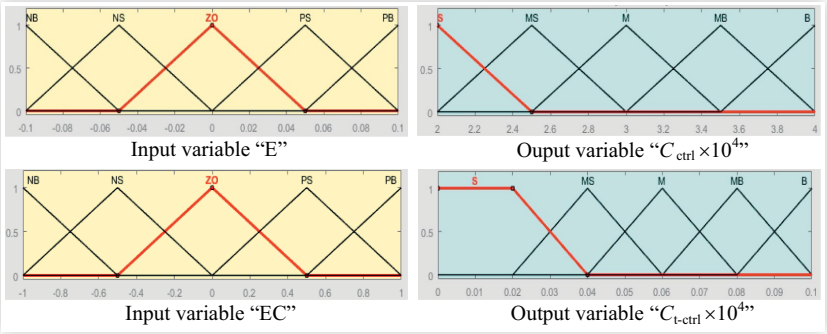
1. Encoding mechanism and initial population: In the FIS's rules, there are 25 control rules that correspond with 25 elements. These 25 elements are then

FIGURE 5 The control model with the OFC.



© Vanliem Nguyen, Renqiang Jiao, Jianrun Zhang

FIGURE 6 Membership functions for input/output variables of the OFC.



© Vanliem Nguyen, Renqiang Jiao, Jianrun Zhang

connected into a string of numbers as a chromosome which is regarded as a vector. Encoding mechanism can shorten the chromosome length of the individuals in a population space to enhance the running speed and to reduce the searching space of the algorithm program. Thus the linguistic variable of two inputs (E and EC) is encoded by the numbers of [NB, NS, ZO, PS, PB] = [0, 1, 2, 3, 4] = $[a_n]_{1\times5}$, and the linguistic variable of the output (u) is encoded by the numbers of [S, MS, M, MB, B] = [5, 6, 7, 8, 9] = $[b_n]_{1\times5}$. Besides the individuals in the initial population are randomly generated. For each gene, the value of that gene is also selected as a random positive integer in the range of $0 \le a_n \le 4$ and $5 \le b_n \le 9$, and the size of the initial population is 100.

2. Objective function and fitness value: In this article, both the minimum RMS_l and DLC_j values described in Equations 18 and 19 are selected as objective functions. To find the minimum value of the objective functions, the fitness value J_1 and J_2 is greatly simplified to calculate the objective functions as follows [10, 16]:

$$J_1 = \frac{1}{\Sigma\alpha_l \mathrm{RMS}_l^2} \quad \text{and} \quad J_2 = \frac{1}{\Sigma\beta_j \mathrm{DLC}_j^2} \qquad \text{Eq. (21)}$$

where J_1 and J_2 are the fitness value of the RMS_l and DLC_j values, α_l is the weight coefficient of the RMS_l value, and β_j is the weight coefficient of the DLC_j value, subscript l refers to the first, second, third, fourth, and fifth wheel axles.

3. Additionally, to avoid the optimal result skewed in the direction of the RMS or DLC values, a weight parameter between J_1 and J_2 for both the CD and CAS methods is proposed to eliminate the bias in selecting the optimal value for FIS's rules as follows:

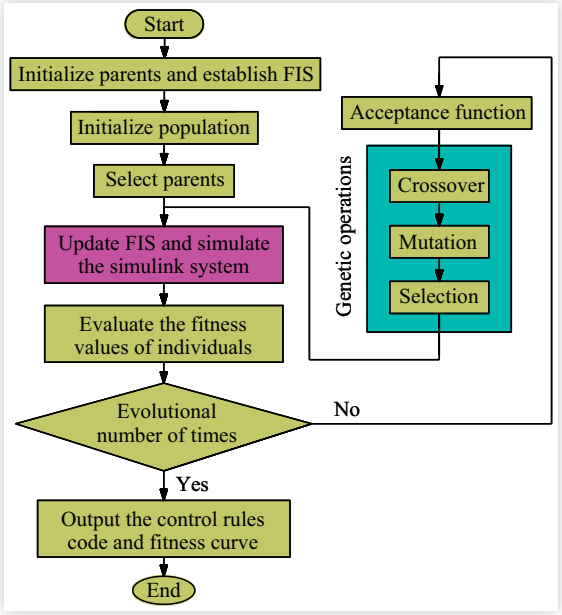
$$\kappa = J_2/J_1 \qquad \text{Eq. (22)}$$

TABLE 1 Major parameters of heavy trucks.

Parameter	Value	Parameters	Value
m_1 (kg)	4,871	$K_{e1r,l}$ (N·m^{-1})	1.1310 × 10^5
m_2 (kg)	27,542	$K_{e2r,l}$ (N·m^{-1})	8.9315 × 10^5
m_{A1} (kg)	584	$K_{e3r,l}$ (N·m^{-1})	7.8807 × 10^5
m_{A2} (kg)	1,554	$K_{v1r,l}$ (N·m^{-1})	1.9009 × 10^5
m_{A3} (kg)	1,314	$K_{v2r,l}$ (N·m^{-1})	15.006 × 10^5
l_1 (m)	3.121	$K_{v3r,l}$ (N·m^{-1})	13.238 × 10^5
l_2 (m)	5.057	$K_{T1r,l}$ (N·m^{-1})	8.9665 × 10^5
l_3 (m)	0.847	K_{Tj} (N·m^{-1})	1.7933 × 10^6
l_4 (m)	3.356	$C_{st1r,l}$ (Ns^2·m^{-2})	0.4127 × 10^4
$l_{5,6}$ (m)	0.661	$C_{st2r,l}$ (Ns^2·m^{-2})	3.2581 × 10^4
l_7 (m)	4.822	$C_{st3r,l}$ (Ns^2·m^{-2})	2.8750 × 10^4
l_8 (m)	4.862	$C_{p1r,l}$ (Ns·m^{-1})	1.2770 × 10^4
$l_{9,10}$ (m)	0.661	$C_{p2r,l}$ (Ns·m^{-1})	2.5539 × 10^4
b_{1r} (m)	1.12	$C_{p3r,l}$ (Ns·m^{-1})	3.3098 × 10^4
b_{1l} (m)	1.08	$C_{T1r,l}$ (Ns·m^{-1})	1.1050 × 10^3
$b_{3r,l}$ (m)	1.10	C_{Tj} (Ns·m^{-1})	2.4140 × 10^3
$b_{T1r,l}$ (m)	1.20	j = 2, 3, ..., 5	

© Vanliem Nguyen, Renqiang Jiao, Jianrun Zhang

FIGURE 7 The flowchart of the GA program.



© Vanliem Nguyen, Renqiang Jiao, Jianrun Zhang

where κ is a constant for both the CD and CAS methods, and it depends on the initial value of J_1 and J_2 with the P.

Therefore, the individuals of the higher fitness values of J_1 and J_2 satisfying κ show that the obtained control rules are better. The resultant individuals are then updated before the evolution process ends, and the optimal individuals can be obtained.

4. Genetic operations: After establishing the initial population and selecting the parents, genetic operations are performed. Herein the crossover probability of 0.95 and a mutation probability of 0.05 are used in 1000 generations. Crossover operation is performed until the population number is doubled and then each individual undergoes the mutation operation which is the process of randomly changing the value of genes in a chromosome with a probability of 0.05. The purpose of mutation is to create new genetic materials into an existing individual and add diversity to the population's genetic characteristics. Finally, through the fitness value of J_1 and J_2, only optimal individuals are selected at the end of each generation to exist in the next generation. For the termination criterion, the limitary generation is used, and the resultant population is then evaluated to determine convergence.

4.3. Optimal Result of the Control Rules

In order to seek the optimal rule in the FIS for both CD and CAS models, assuming that the heavy truck travels under a road surface roughness of road level C at a vehicle velocity of 20 m·s^{-1}, the subsystem model in Figure 5 with the time of 10 s is chosen for simulation. Also based on the simulation result with the P in Table 4, the weight coefficients α_l and β_j of the RMS$_l$ and DLC$_j$ values are calculated by α_{z1} = 0.486, $\alpha_{\phi 1}$, = 0.096, $\alpha_{\theta 1}$ = 0.418 and β_1 = 0.075, β_2 = 0.243, β = 0.231, β_4 = 0.235, β_5 = 0.216, respectively. Then the weight parameter κ calculated through Equation 22 is $\kappa = J_2/J_1 = 8.16$. The error of κ and maximum generation of GA are set to ±0.05 and 1000.

At the completion of the optimal process, only the fitness value of J_1 and J_2 satisfying κ is then plotted in Figure 8. The optimal result in Figure 8a and 8b shows that the maximum fitness value of J_1 and J_2 is respectively obtained through the EG from 760 to the end for CD and 746 to the end for CAS. Therefore, the optimal individuals of the CD and CAS methods can be obtained at the generations of 760 and 746. By recording, the optimal control rules are listed in Tables 2 and 3. They are then used for the OFC to simulate and evaluate the performance of the CD and CAS methods.

5. Result and Discussion

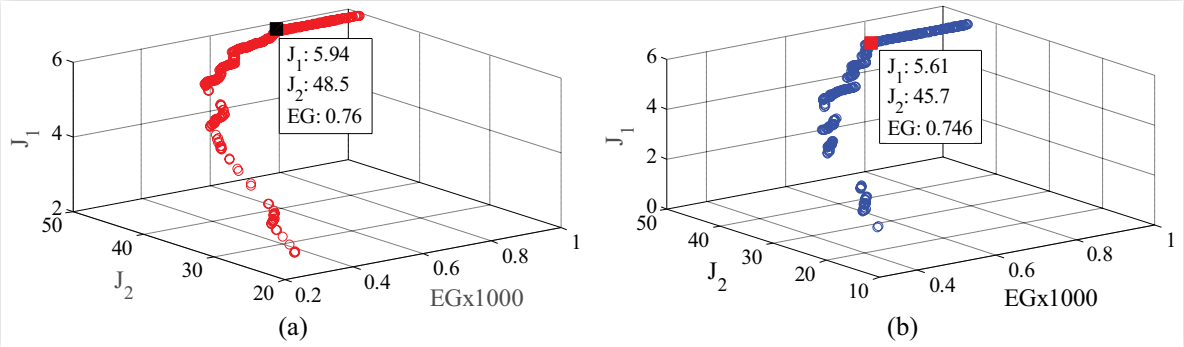
5.1. Under the Effect of the Road Profiles

The purpose of this study is to compare the performance between the CD and CAS methods. Thus based on the reference parameter of the heavy trucks in Table 1, the simulation is performed under the condition of the vehicle travelling on a road surface roughness of road level C and bumpy road surface at v = 20 m·s^{-1}, respectively.

Under the excitation of the road surface roughness: The simulation result of RMS and DLC values of the tractor and wheel axles with the P is listed in Table 4. The result shows that the RMS values of the tractor in the vertical direction and roll angle are significantly great while the RMS value in the pitch angle is small and, thus, the vehicle's ride comfort is strongly affected by the vertical and rolling accelerations. Besides, the DLC value of the second and fourth wheel axles is bigger than other axles. It implies that the effect of the vertical dynamic load of the second and fourth wheel axles on the road damage is large and it should be considered.

Based on the optimal control rules, the control parameter of C_{ctrl} and $C_{t\text{-}ctrl}$ is then simulated to evaluate the performance of the CD and CAS methods. The control result of the acceleration responses of the tractor and maximum dynamic load of the second wheel axle is shown in Figures 9 and 11a. It can be seen that the simulation result with both the CD and CAS

FIGURE 8 The curve of J_1, and J_2 along with the evolutionary generations (EG) for (a) the CD and (b) the CAS.



© Vanliem Nguyen, Renqiang Jiao, Jianrun Zhang

TABLE 2 The optimal rule of the CD.

		EC				
C_{ctrl}		NB	NS	ZO	PS	PB
	NB	B	B	MB	S	S
	NS	MB	M	MS	S	MS
E	ZO	MB	MS	S	MS	M
	PS	MS	S	MS	M	B
	PB	S	MS	MS	M	B

© SAE International

TABLE 3 The optimal rule of the CAS.

		EC				
$C_{t\text{-}ctrl}$		NB	NS	ZO	PS	PB
	NB	B	MB	M	S	S
	NS	MB	MB	M	S	MS
E	ZO	M	M	S	MS	MB
	PS	MS	S	MS	MB	B
	PB	S	MS	MB	MB	B

© SAE International

methods is remarkably reduced in comparison with the P. Also observing Figure 9a, 9b, and 9c, the result shows that the acceleration responses with CD are smaller than with CAS. Contrariwise, the dynamic load of the second wheel axle with CAS is lower than with CD, as seen in Figure 11a. Both the RMS and DLC values are also compared in the same Table 4. The comparison result indicates that the RMS value of the vertical, pitch, and roll vibrations with CD is strongly reduced by 24.2%, 11.4%, and 20%, and with CAS is also clearly decreased by 19.9%, 9.5%, and 17.9% in comparison with P. Besides the DLC value of all the wheel axles with both CD and CAS methods is reduced, especially the maximum DLC value of the second and fourth wheel axles with the CD and CAS methods is smaller by 14.5%, 13.9%, and 18.3%, 17.5% in comparison with P. Thus both the CD and CAS methods not only improve better ride comfort of the tractor but also reduce the road damage.

In addition, the comparison result between the CD and CAS methods also shows that the RMS values with CD are lower than with CAS by 5.6%, 2.2%, and 2.6%, whereas the DLC value with CAS is smaller than with CD on all the wheel axles, especially the maximum DLC value of the second and fourth wheel axles is reduced by 4.5% and 4.0%. Therefore, it can be included that the CD method can improve better ride comfort of the tractor while the CAS method can improve better road friendliness.

Under the excitation of the bumpy road surface: The simulation is also performed under a bumpy road to evaluate the performance of two control methods. The simulation results of the tractor acceleration responses and dynamic load of a third wheel axle are plotted in Figures 10 and 11b. Similar to random excitation, the results also show that the CD method can reduce the tractor's acceleration responses better than the CAS method whereas the road friendliness with CAS is improved better than with CD.

5.2. Under the Effect of the Road Surface Roughness and Vehicle Speeds

To confirm the reliability of the model as well as the above simulation results, other vehicle parameters are unchanged, three different air suspensions of the P, CD, and CAS are then simulated under different conditions of road levels B to E and a velocity range of 2.5 to 30 $m{\cdot}s^{-1}$, respectively. The simulation results of RMS values of the tractor are depicted in Figure 12a, 12b, and 12c. It can be seen that the RMS values with both the CD and CAS methods are remarkably reduced in comparison with P under various road surfaces and vehicle velocities, especially under road levels D and E. Besides the performance of the CD and CAS methods is also clearly reflected in the same Figure 12. All the RMS values with CD are lower than with CAS under different simulation conditions. Therefore, the tractor's ride comfort with CD is better than with CAS.

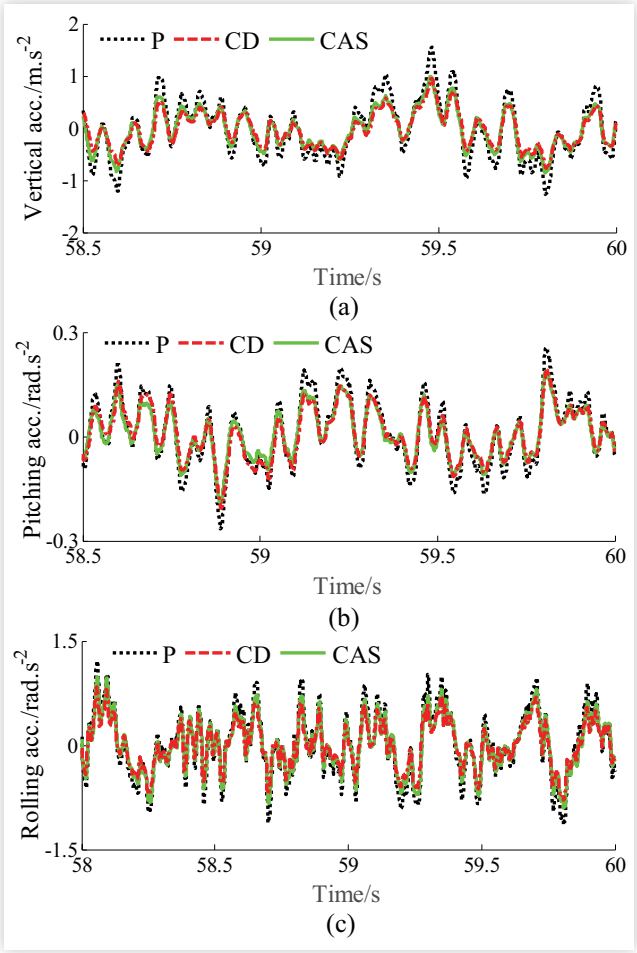
In addition, the control performance of the CD and CAS methods on road friendliness is also evaluated via the DLC value. Based on the DLC result in Table 4, the vertical dynamic loads of the second and fourth wheel axles greatly affect damage to the road surface; therefore, the DLC values of the

TABLE 4 The simulation result of the RMS and DLC values under the road surface of road level C.

Control methods	RMS value			DLC value				
	RMS_{z1} ($m{\cdot}s^{-2}$)	$RMS_{\phi 1}$ ($rad{\cdot}s^{-2}$)	$RMS_{\theta 1}$ ($rad{\cdot}s^{-2}$)	First axle	Second axle	Third axle	Fourth axle	Fifth axle
P	0.5218	0.1022	0.4490	0.0547	0.1771	0.1689	0.1716	0.1571
CD	0.3957	0.0905	0.3591	0.0452	0.1515	0.1450	0.1476	0.1404
CAS	0.4178	0.0925	0.3686	0.0437	0.1446	0.1359	0.1416	0.1225
Reduction (%)								
CD versus P	24.2	11.4	20.0	17.3	14.5	14.1	13.9	10.6
CAS versus P	19.9	9.5	17.9	20.1	18.3	19.5	17.5	22.0
CAS versus CD	−5.6	−2.2	−2.6	3.3	4.5	8.2	4.0	12.7

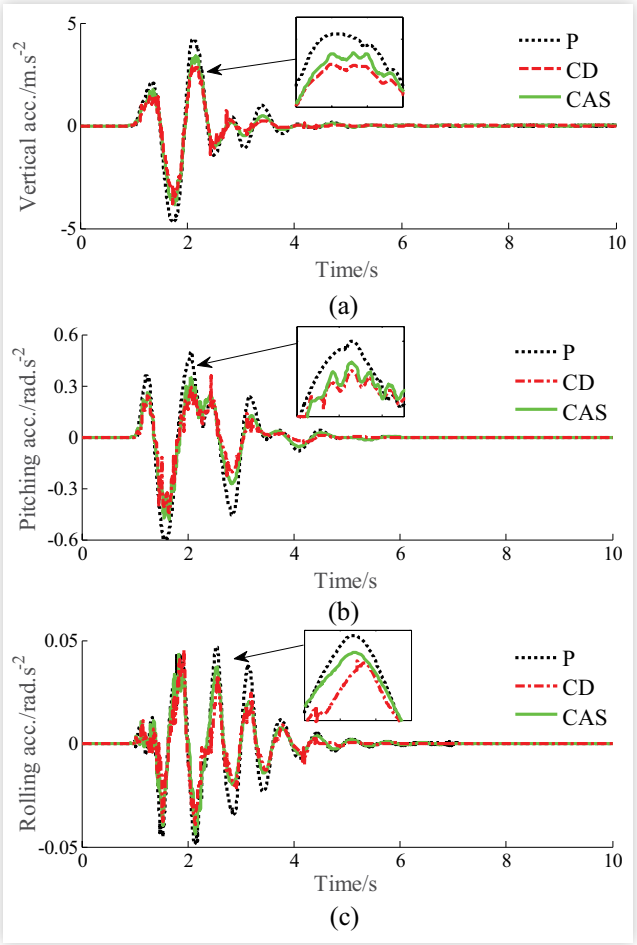
© Vanliem Nguyen, Renqiang Jiao, Jianrun Zhang

FIGURE 9 Acceleration response of (a) vertical, (b) pitching, and (c) rolling vibrations of the tractor under a random road surface.



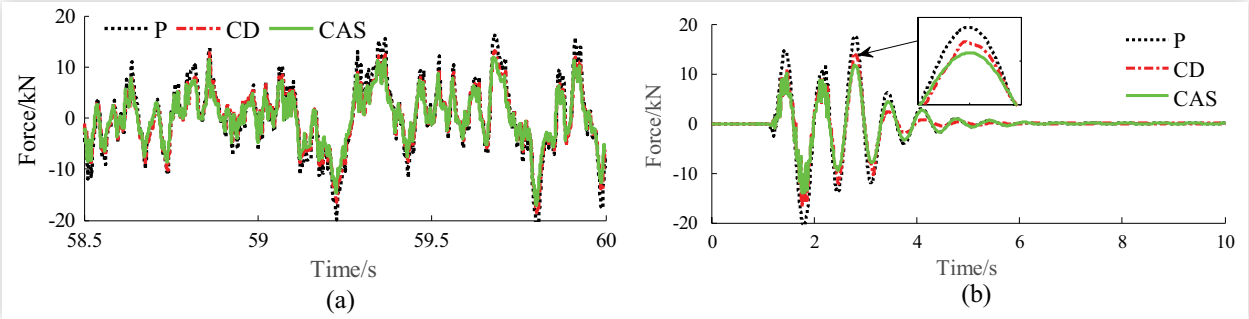
© Vanliem Nguyen, Renqiang Jiao, Jianrun Zhang

FIGURE 10 Acceleration response of (a) vertical, (b) pitching, and (c) rolling vibrations of the tractor under a bumpy road surface.



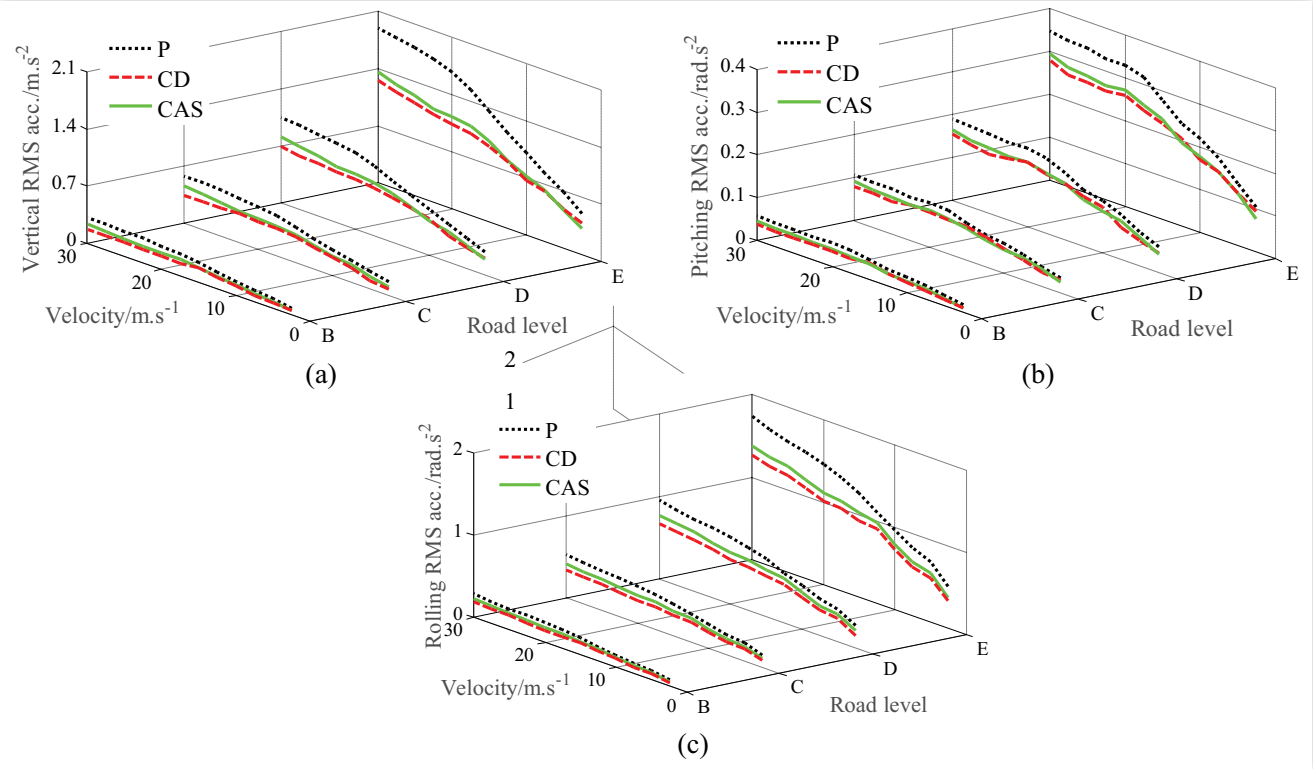
© Vanliem Nguyen, Renqiang Jiao, Jianrun Zhang

FIGURE 11 Tire dynamic force of the second axle (a) under a random surface and (b) of the third axle under a bumpy surface.



© Vanliem Nguyen, Renqiang Jiao, Jianrun Zhang

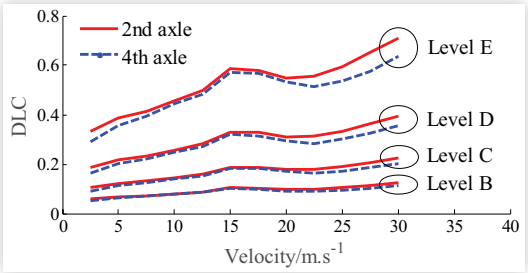
FIGURE 12 The RMS acceleration response of (a) vertical, (b) pitching, and (c) rolling vibrations of the tractor.



© Vanliem Nguyen, Renqiang Jiao, Jianrun Zhang

second and fourth axles are chosen to analyze the result. The simulation results with P in Figure 13 indicate that the DLC values are significantly affected by the vehicle velocities. The DLC values are remarkably increased with increasing vehicle velocity, especially the vehicle velocity from 20.5 to 30 m·s^{-1}. Besides the effect of the vehicle velocity on the DLC values is also different. The DLC value of the second axle is the maximum at vehicle velocity from 15 to 17.5 and 27.5 to 30 m·s^{-1}, whereas the DLC values of the second and fourth axles are greatly reduced at the velocity from 20 to 25 m·s^{-1}. Consequently, this is also the reason that most heavy trucks should travel at this velocity range on the highway to reduce road damage [2, 3, 18].

FIGURE 13 DLC value of the second and fourth wheel axles with the P.

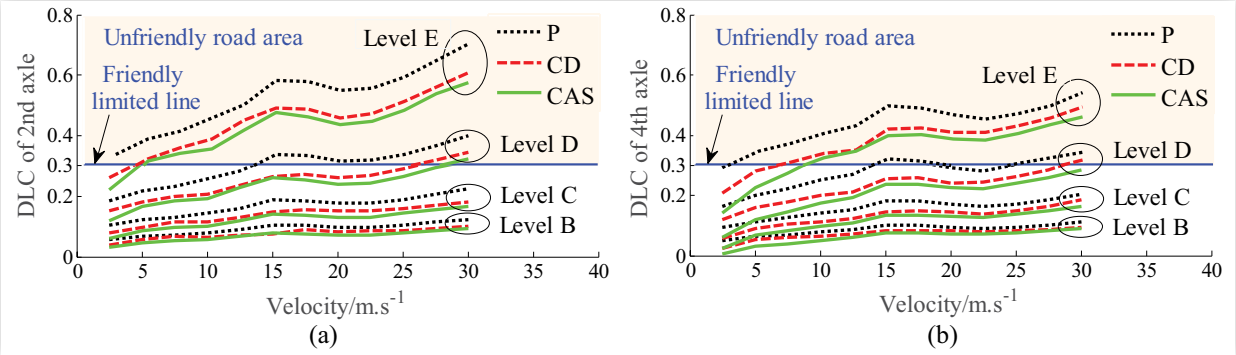


© Vanliem Nguyen, Renqiang Jiao, Jianrun Zhang

Based on the analysis result of DLC value with the P in Figure 13, the DLC values of the second and fourth axles are then used to analyze the performance of the CD and CAS methods on road friendliness. The simulation result is plotted in Figure 14. Observing Figure 14a and 14b, we can see that the DLC values with both CD and CAS methods are remarkably decreased in comparison with the P. Especially under road level D, the tire-road contact of the second and fourth axles with the P can be broken at vehicle velocity over 13.5 m·s^{-1} (DLC > 0.3) [3, 8, 14]; however, it is strongly enhanced at vehicle velocity range over 26 and 29 m·s^{-1} of the second and fourth axles with the CD, and over 27 m·s^{-1} of only the second axle with the CAS. Moreover, the maximum DLC values of the second and fourth wheel axles at a velocity range from 15 to 20 m·s^{-1} are remarkably reduced by both the CD and CAS methods, especially the CAS method.

Moreover, the maximum dynamic load of the second and fourth wheel axles not only affects the durability of the suspension system but also impacts on the road damage, particularly when the excitation frequency of the road coincides with the frequency of suspension system. Consequently, to further enhance the reliability of the vehicle dynamic model as well as the performance of the CAS on the road friendliness, the force-frequency responses of the second and fourth wheel axles in the frequency domain are simulated under the road surface of ISO level C at v = 15 m·s^{-1}, as shown in Figure 15. It can be seen in Figure 15a and 15b that the peak frequencies (the frequencies corresponding to resonant peaks) with the P,

FIGURE 14 The DLC performance on (a) the second and (b) the fourth axles with CD and CAS.



© Vanliem Nguyen, Renqiang Jiao, Jianrun Zhang

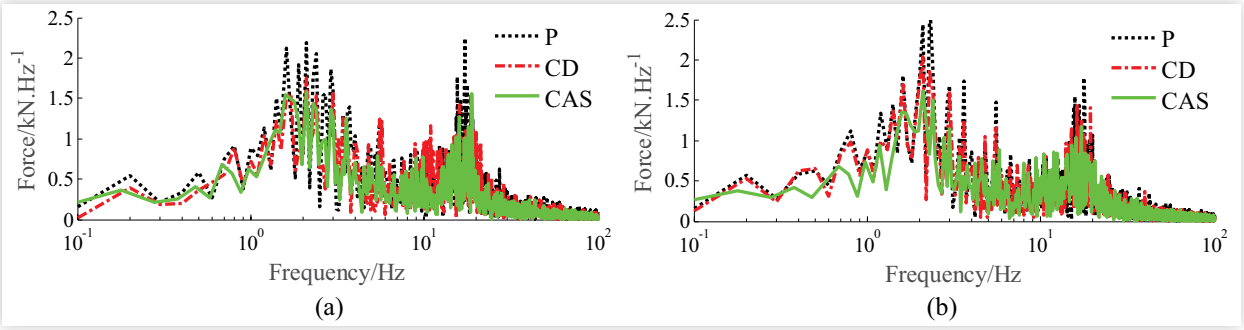
CD, and CAS mainly occur in the range from 1 to 25 Hz, which occurs similarly to commercial vehicles [32]. The spectrum amplitude of the force responses with the CD is lower than with the P; however, the resonant frequencies are mostly unchanged due to the stiffness of the air suspension system with both the CD and P as the same. With the CAS, the spectrum amplitude of the force responses is clearly reduced; concurrently the resonant frequencies are also smaller than both the P and CD. This can be due to the impact of the elastic stiffness of air springs which is changed and depended on the control of the valve in the surge pipe. From the above analysis results, it can be concluded that the tractor's ride comfort is improved by the CD whereas the road friendliness of the wheel axles is improved by the CAS under various road surfaces and velocities.

5.3. Under the Effect of the Vehicle Loads

Three different loading conditions including half loading, full loading, and overloading of the heavy trucks are applied to simulate and compare the performance between the CD and CAS methods under road level C at the vehicle velocity range. The simulation results of the RMS values of the tractor are plotted in Figure 16. Observing Figure 16a, 16b, and 16c, we can see that the RMS values are significantly reduced by both the CD and CAS methods under various loading conditions, particularly the CD. The results also show that the RMS values are greatly influenced by the velocity and loading conditions of the vehicle. Figure 16a and 16b indicate that both the RMS values of the vertical and pitching vibrations under the half-loading condition are smaller under full loading and overloading conditions at a velocity range below 20 $m{\cdot}s^{-1}$; conversely, their RMS values are quickly increased under the half-loading condition at a velocity range over 20 $m{\cdot}s^{-1}$. Figure 16c indicates that the rolling RMS value under the half-loading condition is higher than both full loading and overloading conditions under various vehicle velocities. Thus the tractor's ride comfort is greatly reduced under the half-loading condition, especially the tractor's roll vibration.

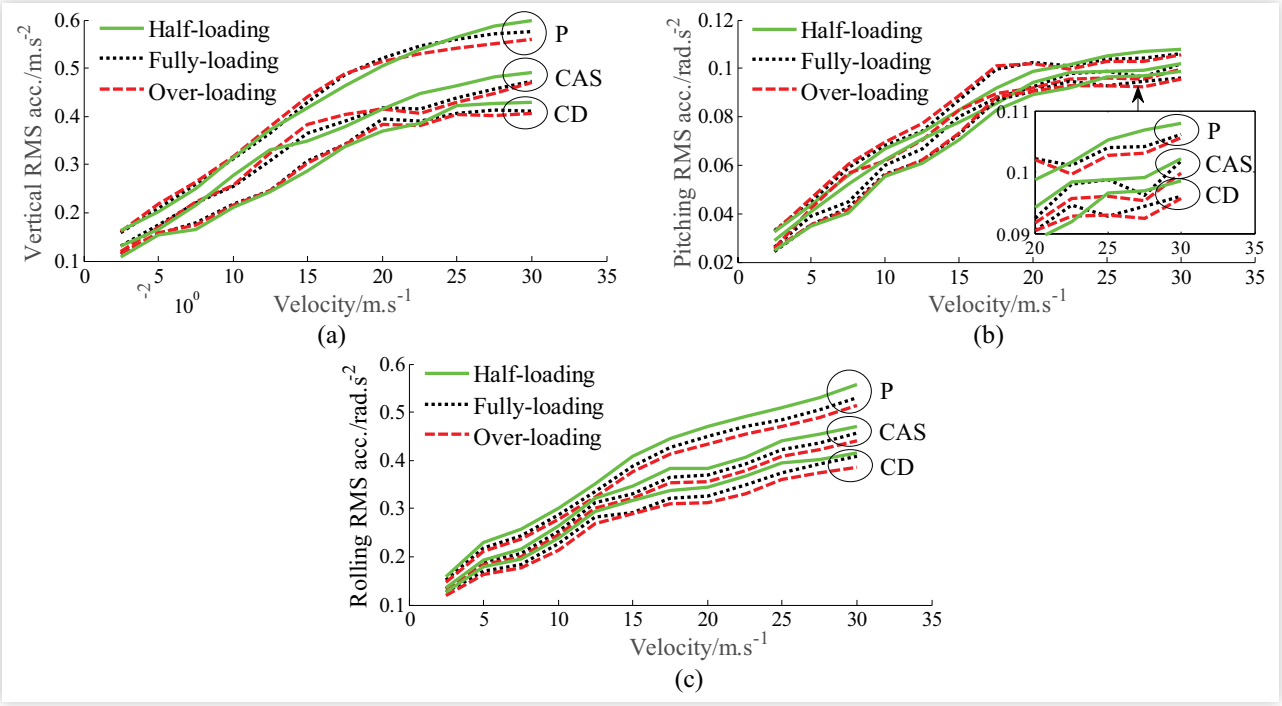
The simulation result of the DLC values of the second and fourth wheel axles under the different loading conditions is plotted in Figure 17a and 17b. The result demonstrates that the DLC values strongly depend on the loading conditions. The DLC values are strongly increased under the half-loading condition and significantly reduced under the overloading condition in comparison with the full loading condition. This implies that the road friendliness of heavy trucks is improved when the vehicle load is increased and vice versa. Besides the DLC values of the second and fourth wheel axles with both the CD and CAS is smaller than with the P under all the loading conditions, especially the CAS. Consequently, based on the above analysis results, it can be concluded that the

FIGURE 15 The force-frequency response on (a) the second and (b) the fourth wheel axles.



© Vanliem Nguyen, Renqiang Jiao, Jianrun Zhang

FIGURE 16 RMS acceleration response of (a) vertical, (b) pitching, and (c) rolling vibrations of the tractor under the different loading conditions.



© Vanliem Nguyen, Renqiang Jiao, Jianrun Zhang

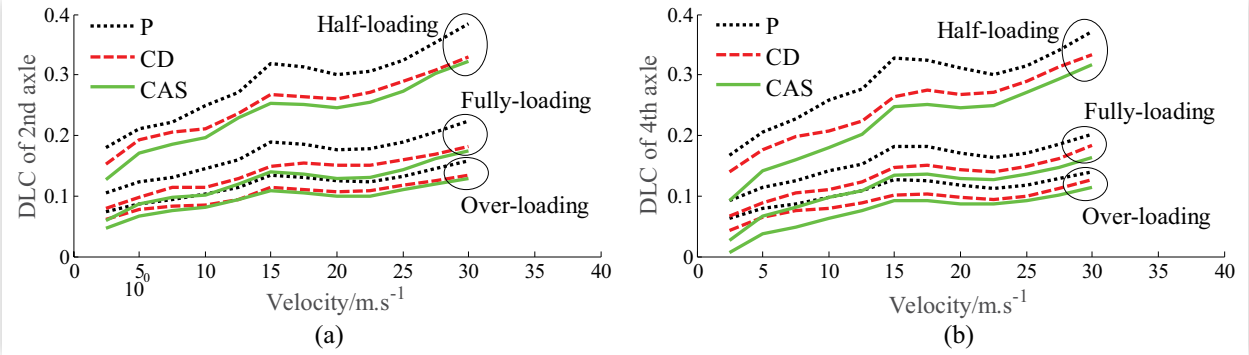
tractor's ride comfort is improved by the CD whereas the road friendliness is improved by the CAS under the different loading conditions.

6. Conclusions

A 3D nonlinear dynamic model of the five-axle heavy trucks equipped with the air suspension system is studied and controlled. The performance of the CD and the CAS methods using the OFC is analyzed through the object functions of the RMS and DLC values. The results are summarized as follows:

1. A new optimal method for the FLC's control rules based on the GA, which is known as a multi-objective optimal algorithm with wide search range and short search time, is successfully developed and applied for the air suspension system of the heavy trucks.
2. Under various operating conditions, the ride comfort and the road friendliness of the heavy trucks are remarkably improved with both the CD and CAS methods in comparison with the P method, especially under the poor road surfaces of road levels D and E.
3. The DLC value of the wheel axles with the CAS method is considerably reduced in comparison with the CD method, especially the maximum DLC value

FIGURE 17 The control performance on the DLC values under the different loading conditions.



© Vanliem Nguyen, Renqiang Jiao, Jianrun Zhang

of the second and fourth wheel axles at the vehicle velocity range from 15 to 20 $m \cdot s^{-1}$ and under the different loading conditions. Moreover, the spectrum amplitude of the force-frequency response with the CAS method is also lower than the CD method in the frequency domain. Therefore, the CAS method is better than the CD method to reduce the impact of the tire dynamic load on the road damage and improve the road friendliness; conversely, based on the RMS result of the tractor, the CD method is better than the CAS method to improve the tractor's ride comfort.

Acknowledgments

This work has been supported by the National Key Research and Development Plan (No. 2019YFB2006402); Hubei Polytechnic University Teaching and Research Projects (No. 19XJK17R).

Abbreviations

CAS - Controlled Air Spring
CD - Controlled Damping
DLC - Dynamic Load Coefficient
FIS - Fuzzy Inference System
FLC - Fuzzy Logic Control
GA - Genetic Algorithm
ISO - International Organization for Standardization
J - Fitness value
MR - Magneto-Rheological
OFC - Optimal Fuzzy Control
P - Passive
PSD - Power Spectral Density
RMS - Root Mean Square

References

1. Xie, Z., Wong, K., Jing, Z., Tao, X. et al., "A Noise-Insensitive Semi-Active Air Suspension for Heavy-Duty Vehicles with an Integrated Fuzzy-Wheelbase Preview Control," *Mathematical Problems in Engineering* 2013(8):1-12, 2013, https://doi.org/10.1155/2013/121953.
2. Georgios, T., Charles, W., and Emanuele, G., "Hybrid Balance Control of a Magnetorheological Truck Suspension," *Journal of Sound and Vibration* 317:514-536, 2008, https://doi.org/10.1016/j.jsv.2008.03.040.
3. Liem, N., Zhang, J., Le, V., Jiao, R. et al., "Performance Analysis of Air Suspension System of Heavy Truck with Semi-Active Fuzzy Control," *Journal of Southeast University* 33(2):159-165, 2017, https://doi.org/10.3969/j.issn.1003-7985.2017.02.006.
4. Kulakowski, B., Streit, D., Wollyung, R., and Kenis, W., "A Study of Dynamic Wheel Loads Conducted Using a Four-Post Road Simulator," in *Proceedings of the 4th International Symposium on Heavy Vehicle Weights and Dimensions*, Transportation Research Institute, University of Michigan, Ann Arbor, MI, 301-307, 1995.
5. Berg, M., "A Three-Dimensional Air Spring Model with Friction and Orifice Damping," in *Proceedings of the 16th IAVSD Symposium, the Dynamics of Vehicles on Roads and on Tracks*, South Africa, Vol. 33, 528-539, 1999.
6. Nguyen, V., Zhang, J., Le, V., and Jiao, R., "Vibration Analysis and Modeling of an Off-Road Vibratory Roller Equipped with Three Different Cab's Isolation Mounts," *Shock and Vibration* 2018:1-17, 2018, https://doi.org/10.1155/2018/8527574.
7. Sundvall, P., "Comparisons between Predicted and Measured Ride Comfort in Trains - A Case Study on Modeling," TRITAFKT Report, Division of Railway Technology, Department of Vehicle Engineering, Royal Institute of Technology, Stockholm, Sweden, 2001.
8. Buhari, R., Rohani, M., and Abdullah, M., "Dynamic Load Coefficient of Tyre Forces from Truck Axles," *Applied Mechanics and Materials* 405-408:1900-1911, 2013, https://doi.org/10.4028/www.scientific.net/amm.405-408.1900.
9. Chen, Y., He, J., Li, X. et al., "Integrated Performance Optimum Design of Heavy Truck Air Suspension Based on Fuzzy Control," *Journal of Southeast University* 38(2):319-323, 2008.
10. Nguyen, V., Zhang, J., and Yang, X., "Low-Frequency Performance Analysis of Semi-Active Cab's Hydraulic Mounts of an Off-Road Vibratory Roller," *Shock and Vibration* 2019:1-15, 2019, https://doi.org/10.1155/2019/8725382.
11. Kasemi, B., Muthalif, A.G.A., Rashid, M.M., and Fathima, S., "Fuzzy-PID Controller for Semi-Active Vibration Control Using Magnetorheological Fluid Damper," *Procedia Engineering* 41:1221-1227, 2012, https://doi.org/10.1016/j.proeng.2012.07.30428.
12. Nguyen, T., "A Novel Semi-Active Magnetorheological Mount for Vibration Isolation," Ph.D. thesis, The University of Toledo, Toledo, OH, 2009.
13. Muthalif, A., Kasemi, B., Nordin, D., and Rashid, M., "Semiactive Vibration Control Using Experimental Model of Magnetorheological Damper with Adaptive Fuzzy-PID Controller," *Smart Structures and Systems* 20(1):85-97, 2017, https://doi.org/10.12989/sss.2017.20.1.085.
14. Cole, D. and Cebon, D., "Truck Suspension Design to Minimize Road Damage," *Proceedings of the Institute of Mechanical Engineers, Part D. Journal of Automobile Engineering* 210:95-107, 1996, https://doi.org/10.1243/pime_proc_1996_210_251_02.
15. Nguyen, S., Nguyen, Q., and Choi, S., "A Hybrid Clustering Based Fuzzy Structure for Vibration Control-Part 2: An Application to Semiactive Vehicle Seat-Suspension System," *Mechanical System Signal Processing* 56-57:288-301, 2015, https://doi.org/10.1016/j.ymssp.2014.04.021.

16. Wang, W., Song, Y., Xue, Y., Jin, H. et al., "An Optimal Vibration Control Strategy for a Vehicle's Active Suspension Based on Improved Cultural Algorithm," *Applied Soft Computing Journal* 28:167-174, 2015, https://doi.org/10.1016/j.asoc.2014.11.047.

17. Chen, Y., Wang, Z., Qiu, J., and Huang, Z., "Hybrid Fuzzy Skyhook Surface Control Using Multi-Objective Microgenetic Algorithm for Semi-Active Vehicle Suspension System Ride Comfort Stability Analysis," *Journal of Dynamic Systems Measurement & Control* 134(4):1-14, 2012, https://doi.org/10.1115/1.4006220.

18. Le, V., Zhang, J., Liu, X., and Wang, Y., "Nonlinear Dynamic Analysis of Interaction between Vehicle and Road Surfaces for 5-Axle Heavy Truck," *Journal of Southeast University* 27(4):405-409, 2011, https://doi.org/10.3969/j.issn.1003-7985.2011.04.012.

19. Presthus, M., "Derivation of Air Spring Model Parameters for Train Simulation," M.S. thesis, Lulea University of Technology, 2002.

20. Captain, M., Boghani, B., and Wormley, N., "Analytical Tire Models for Dynamic Vehicle Simulation," *Vehicle System Dynamics* 8(1):1-32, 1979, https://doi.org/10.1080/00423117908968566.

21. Killner, R., "Pneumatic Tire Model for Aircraft Simulation," *Journal of Aircraft* 19(10):851-857, 1982, https://doi.org/10.2514/3.44786.

22. Shi, X. and Cai, C., "Simulation of Dynamic Effects of Vehicles on Pavement Using a 3D Interaction Model," *Journal of Transportation Engineering* 135(10):736-744, 2009, https://doi.org/10.1061/(ASCE)TE.1943-5436.0000045.

23. Song, C., Zhao, Y., and Wang, L., "Tri-Objective Co-Evolutionary Algorithm and Application of Suspension Parameter Design Based on Lizard Behavior Bionics," *Journal of Mechanical Science and Technology* 28(12):4857-4867, 2014, https://doi.org/10.1007/s12206-014-1106-2.

24. International Organization for Standardization, ISO 8068, "Mechanical Vibration-Road Surface Profiles-Reporting of Measured Data," 1995.

25. International Organization for Standardization, "Mechanical Vibration and Shock-Evaluation of Human Exposure to Whole Body Vibration-Part 1: General Requirements," Tech. Rep. ISO 2631-1:1997, ISO, Geneva, Switzerland, 1997.

26. Lu, Y., Yang, S., Li, S., and Chen, L., "Numerical and Experimental Investigation on Stochastic Dynamic Load of a Heavy Duty Vehicle," *Applied Mathematical Modelling* 34(10):2698-2710, 2010, https://doi.org/10.1016/j.apm.2009.12.006.

27. Chen, Y., He, J., King, M., Chen, W. et al., "Effect of Driving Conditions and Suspension Parameters on Dynamic Load-Sharing of Longitudinal-Connected Air Suspensions," *Science China Technological Sciences* 56(3):666-676, 2012.

28. Kulakowski, B., Husted, D., and Streit, D., "Models of Dynamic Load Coefficient for a Two-Axle Truck Obtained from Road Simulator Data," *International Journal of Heavy Vehicle System* 3(1-4):293-305, 1996, https://doi.org/10.1504/IJHVS.1996.054566.

29. Mamdani, E. and Assilian, S., "An Experiment in Linguistic Synthesis with a Fuzzy Logic Controller," *International Journal Human-Computer Studies* 51:135-147, 1999, https://doi.org/article no.ijhc.1973.0303.

30. Nariman, Z., Salehpour, M., Jamali, A., and Hanghgoo, E., "Pareto Optimization of a Five-Degree of Freedom Vehicle Vibration Model Using a MUGA," *Engineering Applications of Artificial Intelligence* 23(4):543-551, 2010, https://doi.org/10.1016/j.engappai.2009.08.008.

31. John, H., Michael, G., and Gregory, D., "Multi-Objective Control Optimization for Semi-Active Vehicle Suspensions," *Journal of Sound and Vibration* 330:5502-5516, 2011, https://doi.org/10.1016/j.jsv.2011.05.036.

32. Gillespie, T. and Karramihas, S., "Simplified Models for Truck Dynamic Response to Road Inputs," *International Journal Vehicle System* 7(1):52-63, 2000, https://doi.org/10.1504/IJHVS.2000.004450.

© 2020 Vanliem Nguyen, Renqiang Jiao, Jianrun Zhang. Published by SAE International. This Open Access article is published under the terms of the Creative Commons Attribution License (http://creativecommons.org/licenses/by/4.0/), which permits distribution, and reproduction in any medium, provided that the original author(s) and the source are credited.

Positions and opinions advanced in this work are those of the author(s) and not necessarily those of SAE International. Responsibility for the content of the work lies solely with the author(s).